Fault interaction and stresses along broad oceanic transform zone: Tjörnes Fracture Zone, north Iceland

Catherine Homberg, Françoise Bergerat, Jacques Angelier, Sébastien Garcia

Fault interaction and stresses along broad oceanic transform zone: Tjörnes Fracture Zone, north Iceland

C. Homberg,[1] F. Bergerat,[1] J. Angelier,[2] and S. Garcia[3]

Received 16 October 2008; revised 18 July 2009; accepted 2 September 2009; published 22 January 2010.

[1] Transform motion along oceanic transforms generally occurs along narrow faults zones. Another class of oceanic transforms exists where the plate boundary is quite large (~100 km) and includes several subparallel faults. Using a 2-D numerical modeling, we simulate the slip distribution and the crustal stress field geometry within such broad oceanic transforms (BOTs). We examine the possible configurations and evolution of such BOTs, where the plate boundary includes one, two, or three faults. Our experiments show that at any time during the development of the plate boundary, the plate motion is not distributed along each of the plate boundary faults but mainly occurs along a single master fault. The finite width of a BOT results from slip transfer through time with locking of early faults, not from a permanent distribution of deformation over a wide area. Because of fault interaction, the stress field geometry within the BOTs is more complex than that along classical oceanic transforms and includes stress deflections close to but also away from the major faults. Application of this modeling to the 100 km wide Tjörnes Fracture Zone (TFZ) in North Iceland, a major BOT of the Mid-Atlantic Ridge that includes three main faults, suggests that the Dalvik Fault and the Husavik-Flatey Fault developed first, the Grismsey Fault being the latest active structure. Since initiation of the TFZ, the Husavik-Flatey Fault accommodated most of the plate motion and probably persists until now as the main plate structure. **Citation:** Homberg, C., F. Bergerat, J. Angelier, and S. Garcia (2010), Fault interaction and stresses along broad oceanic transform zone: Tjörnes Fracture Zone, north Iceland, *Tectonics*, *29*, TC1002, doi:10.1029/2008TC002415.

1. Introduction

[2] Geophysical investigations of the oceanic floors have emphasized that spreading ridges, separating both fast and slow divergent plates, commonly show en echelon distribution [e.g., *Lonsdale*, 1989; *Sempéré et al.*, 1995; *Small et al.*, 1999; *Bandy and Hilde*, 2000]. The linkage between two offset ridges may evolve through overlap between ridge segments or through sliding along transform fault. Large efforts have been done to understand the necessary conditions for development of transform faults. Several mechanisms has been advanced involving old continental weakness zones [*Wilson*, 1965], upper mantle negative thermal anomalies [*Bonatti*, 1996] or stress concentration [*Pollard and Aydin*, 1984; *Gudmundsson and Homberg*, 1999].

[3] Most oceanic transforms are narrow fault zones and are typically 10–30 km wide [*Fox and Gallo*, 1986]. Some of them escape this rule, being much wider. This is the case of the Romanche (Mid-Atlantic Ridge), Andrew Bain (Southwest Indian ridge) and Tjörnes fractures zones (Mid-Atlantic Ridge), with widths up to hundreds kilometers. Such broad oceanic transforms (BOTs) are thought to develop in an abnormally thick and cold lithosphere [*Mauduit and Dauteuil*, 1996; *Ligi et al.*, 2002]. The mechanism of the BOTs is poorly understood and major ambiguities exist. To understand the development of such zones, crucial questions can be addressed as follows. (1) Do the individual faults of the BOTs represent permanent major plate boundary structures with equivalent slip rates, or does a master fault absorb most of the plate motion and occasionally triggers slip on the other faults? (2) What are the factors responsible for the complex stress state along the BOTs? (3) Why do strike-slip and transform-parallel normal faults [*Ligi et al.*, 2002] coexist in the BOTs, as they also do in more common oceanic transforms [e.g., *Fox and Gallo*, 1986; *Gudmundsson*, 1993; *Dziak et al.*, 2000]?

[4] To help answering these questions, this paper presents a numerical modeling that helps to understand the evolution of the Tjörnes Fracture Zone (TFZ), a typical BOT of the northern Mid-Atlantic Ridge. We show that the faulting pattern in the crust controls the stress state and the slip distribution along the individual faults of the TFZ. Our model also suggests that distributed strike slip is not a long-lived mechanism; the finite width of a BOT results from slip transfer through time with locking of early faults, rather than from a permanent distribution of deformation over a wide area.

2. Tjörnes Fracture Zone

2.1. Oceanic Fracture Zone

[5] The Tjörnes Fracture Zone (TFZ), a major transform fault of the Mid-Atlantic Ridge (Figure 1), is approximately

[1] ISTeP, UMR 7193, Université Pierre et Marie Curie, CNRS, Paris, France.
[2] Géosciences Azur, UMR 6526, UNSA, UPMC, IRD, Observatoire Océanologique, CNRS, Villefranche-sur-Mer, France.
[3] Institut für Geologische Wissenschaften, Freie Universität Berlin, Berlin, Germany.

0278-7407/10/2008TC002415$12.00

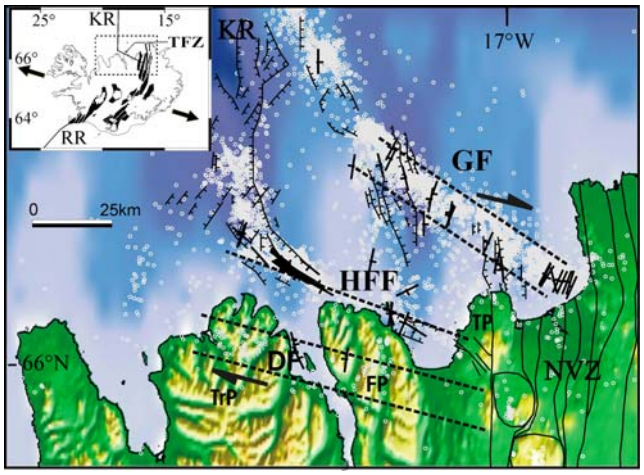

Figure 1. Main structures of the Tjörnes Fracture Zone (TFZ). Thin solid lines denote faults inferred from seismic reflection or observations on land. Barbed lines denote faults with significant vertical movement. Thick solid lines with single bar indicating dip direction denote active strike-slip faults, some of them showing moderate vertical movement (see text for details). Dashed lines denote trend of the Dalvik Fault (DF), Husavik-Flatey Fault (HFF), and Grimsey Fault (GF). White dots denote earthquakes. NVZ, KR, TFZ, and RR are Northern Volcanic Zone, Kolbeinsey Ridge, Tjörnes Fracture Zone, and Reykjanes Ridge, respectively. Thin lines in the NVZ indicate limits of volcanic zones. TrP, FP, TP, Tröllaskagi, Flateyjarskagi, and Tjörnes peninsulas. Faults and earthquakes are after *McMaster et al.* [1977], *Rögnvaldsson et al.* [1998], and *Dauteuil et al.* [2002]. Inset shows the plate configuration with plate separation after *DeMets et al.* [1994].

120 km long and 70 km wide oceanic fracture zone. It trends WNW–ESE (N120°E), thus being oblique at angle of 10–15° with the N107°E direction of plate divergence [*DeMets et al.*, 1994]. The TFZ connects the offshore Kolbeinsey ridge to the onshore rift of Northeast Iceland (Figure 1). Spreading across the Kolbeinsey ridge began between 24 Ma [*Vogt et al.*, 1980; *Kodaira et al.*, 1998] and 9.5 Ma [*Grønlie et al.*, 1979]. However, the development of the TFZ as a right-lateral transform zone is younger because the present-day locus of accretion in Northern Iceland along the Northern Volcanic Zone results from an eastward jump of the Icelandic rift at about 7–9 Ma [*Saemundsson*, 1974]. Recent radiometric dating assigned a maximum age of 8.5 Ma to this rift jump [*Garcia et al.*, 2003], which is thought to be related to the westward displacement of the plate boundary with respect to the Icelandic hot spot [*Burke et al.*, 1973]. The large width of the TFZ may be explained by the high regional heat flow and low strength of the lithosphere due to the occurrence of the hot spot [*Dauteuil et al.*, 2002].

[6] Oceanic accretion in Iceland occurred simultaneously along the Skagafjördur paleorift to the west and the Northern Volcanic Zone to the east between 8 and 8.5 to 3 Ma [*Garcia et al.*, 2003], thus rift jump cannot be considered instantaneous. Dikes being 8.1 ± 0.7 Myr old, strike parallel to the TFZ suggesting the TFZ already existed at this time. It is thus likely that the TFZ appeared between 8.5 and 8 Ma that is since the beginning of the rift jump. The average opening rate of the Kolbeinsey ridge since 12–13 Ma is 2 cm/yr [*Vogt et al.*, 1980], a value close to the present-day rate of opening across the Icelandic rift of 1.8 cm/yr [*DeMets et al.*, 1994]. Accretion along the Northern Volcanic Zone was first asymmetrical with a deficit on the western side [*Garcia et al.*, 2003]. As a consequence, it is likely that the slip rate along the TFZ was much less than 2 cm/yr at the beginning of the transform activity, and later progressively increased up to its present-day value.

2.2. Major Structures of the TFZ

[7] Most of the seismic activity in Northern Iceland occurs in the TFZ. Earthquakes along the TFZ may reach magnitude of 7.1 and their maximum 10–12 km depth decreases close to the ridge axis [*Einarsson*, 1991; *Rögnvaldsson et al.*, 1998]. The earthquake distribution reveals three active lineaments or fault zones, which are from north to south the Grimsey fault (GF), the Husavik-Flatey Fault (HFF) and the Dalvik Fault (DF). The Dalvik Fault is by far less active than the other two lineaments (Figure 1). The GF, HFF, and DF strike N132°E, N122°E, and N117°E, respectively. In details, the Grimsey and Dalvik lineaments mainly consist of en échelon N–S left-lateral seismic faults, whereas the displacement along the N122°E Husavik-Flatey fault occurs on WNW–ESE dextral faults [*Rögnvaldsson et al.*, 1998]. Small grabens running along the onshore and offshore trace of the HFF [*Johnsson*, 1974; *Saemundsson*, 1974; *Flovenz and Gunnarsson*, 1991; *Garcia and Dhont*, 2005] and the presence of significant normal component of seismic fault motion along the GF [*Rögnvaldsson et al.*, 1998] indicate limited extension within the TFZ (Figure 1). These grabens are generally interpreted in terms of fault wedge or pull-apart basin related to strike-slip fault tectonic activity [*Riedel et al.*, 2001]. NNW–SSE normal faults are also well developed between the HFF and the GF [*McMaster et al.*, 1977; *Riedel et al.*, 2001]. Despite this complexity, and although fault offset data are few because most of the transform zone is located offshore, geological evidence leads to consider the TFZ as a genuine right-lateral transform fault zone, not an overlapping spreading center between two rifts segments. First, pull-apart basins between right-stepping fault segments and push-up structures between left-stepping segments clearly indicate the strike-slip nature of the 10 km long onland trace of the HFF and its right-lateral sense of motion [e.g., *Garcia and Dhont*, 2005]. Second, the focal mechanisms of earthquakes indicate dominant strike-slip components of motion along the DF, HFF, and GF, and a present-day stress regime of prevailing strike-slip type despite complexity [*Garcia et al.*, 2002; *Angelier et al.*, 2004].

[8] Because of the absence of clear geological marker, whether the DF, HFF, and GF developed simultaneously or not still remains unknown. Regarding the slip amount along each of these three faults, the HFF, which is generally

regarded as the main plate boundary structure of the TFZ, is marked onland as a geomorphological feature over a distance of 25 km across the Tjörnes peninsula and by a 3–5 km wide zone of intense deformation [e.g., *Fjäder et al.*, 1994; *Garcia and Dhont*, 2005]. The minimum cumulative right-lateral slip along the HFF is 5–10 km or 20 km and may be as large as 60 km [*Saemundsson*, 1974; *Young et al.*, 1985] whereas its vertical displacement is larger than 200 m and may reach 1400 m [*Gudmundsson et al.*, 1993]. The DF is thought to have absorbed little displacement because of its discrete onland expression. The GF, which is almost exclusively an offshore structure, shows a significant present-day seismic activity.

3. Stress Distribution in the Tjörnes Fracture Zone

[9] In this section, we describe the modern and past stress fields along the TFZ based on the inversion of earthquake focal mechanisms [*Garcia et al.*, 2002; *Angelier et al.*, 2004] and fault-slip data collected in lava piles at least 7 Myr old [*Bergerat et al.*, 1990, 1992; *Angelier et al.*, 2000; *Bergerat et al.*, 2000; *Garcia et al.*, 2002]. The stress data will be later compared with the results of numerical modeling. We then examine the relation between this stress field and the main tectonic features of the TFZ.

3.1. Modern Stresses

[10] The first-order modern stress state of the TFZ was obtained through a global inversion of all earthquakes recorded within the TFZ between 1991 and 1999 [*Angelier et al.*, 2004]. 67% of the earthquakes correspond to a strike-slip regime with the maximal horizontal stress (S_{Hmax}) trending N155°E and the minimal horizontal stress (S_{Hmin}) trending N065°E. The remaining earthquakes belong to a second, minor, strike-slip regime with S_{Hmax} striking N060°E. The minor regime is not directly representative of the main activity of the TFZ and probably derived from the main one through principal stress permutation. Focusing on the main regime, *Angelier et al.* [2004] found that within the TFZ S_{Hmin} trends at an angle of 40° with respect to the direction of plate divergence, which led them to conclude that stresses may be severely deflected along major transform faults like the TFZ.

[11] The modern stress trajectories within the TFZ are not known, but comparison between the global inversion of *Angelier et al.* [2004] and the local inversion of *Garcia et al.* [2002] suggests that stresses vary within the plate boundary. By selecting the 1995–1997 earthquakes within a 70 × 30 km box around the HFF, *Garcia et al.* [2002] showed that the mechanisms driving faulting near the HFF are complex and include a variety of substates of stress (Figure 2c). First, both strike slips and normal slips coexist, although the first ones represent 70% of the seismic activity. Second, accounting for all earthquakes requires more than a single stress state, which reveals heterogeneity in the stress field within the selected crust volume. The inversions revealed significant variation in the S_{Hmax} azimuth within the range between N130°E and N170°E. Among the normal focal mechanisms, 26% reflect a previously undetected normal stress regime with S_{Hmax} trending N030°E–N040°E, a direction almost perpendicular to the trend of the HFF.

[12] Whereas the modern stresses along the HFF are rather well constrained, less information is available for the other two faults, DF and GF. Relocalization of earthquakes along the GF showed left-lateral slip on N–S faults [*Rögnvaldsson et al.*, 1998]. Although a stress state cannot be reconstructed based on the sole consideration of such faults, this observation suggests that S_{Hmax} is deviated anticlockwise relative to the N–S direction expected from plate divergence, and thus should trend approximately NW–SE. Determining the accurate geometry of the modern crustal stress field within the TFZ would require to define a gridding scheme of the TFZ with boxes in which the stress field is homogeneous and to perform an inversion in each box. Such a study has not been done up to now. However, the following aspects of the present-day seismotectonic stress regimes within the TFZ emerge from existing studies and the present analysis:

[13] 1. The modern stresses are heterogeneous, as illustrated by the difference between the stresses deduced from the inversion of the whole seismicity in the TFZ [*Angelier at al.*, 2004] and the local reconstruction [*Garcia et al.*, 2002].

[14] 2. A large number of earthquakes indicate a NNW–SSE to NW–SE trending S_{Hmax}.

[15] 3. At a local scale within the central part of the TFZ, S_{Hmax} is clearly deflected both anticlockwise and clockwise, presumably as an effect of perturbations around major faults. These deflections result in local stress states with S_{Hmax} trending N145°E and N035°E on average. These oblique stress azimuths have been clearly evidenced around the HFF, but may exist elsewhere.

3.2. Paleostresses and Tectonic Structures of the TFZ

[16] The past TFZ stress field is known from inversion of secondary faults affecting lavas that are at least 7 Myr old [*Bergerat et al.*, 1990, 1992; *Angelier et al.*, 2000; *Bergerat et al.*, 2000; *Garcia et al.*, 2002]. To perform statistical analysis of the paleostress results, we gathered all this brittle tectonic information within a single database including a total of 287 stress tensors. Examining the trend distribution of stress axes leads us to present the following conclusions. First, the range of S_{Hmax} azimuths is wide (Figure 2a). Moreover, some stress tensors (32.3%) exhibit trends that cannot induce dextral shear along the TFZ. *Bergerat et al.* [2000] concluded that these TFZ-incompatible stress states are derived from the TFZ-compatible ones trough permutation of the principal stress axes. Because we are interested on stresses responsible for the TFZ activity, we do not focus on these stress permutations. Discarding these 'abnormal' stress states to concentrate on the major ones, the four main peaks of S_{Hmax} azimuths are N000°–010°E (18%), N120°–130°E (13%), N170°–180° (16%) and N020°–030°E (14%). 74% of the data show anticlockwise deviation of S_{Hmax} trends relative to the N010°–020°E trend that could be expected from plate divergence, whereas 14% show

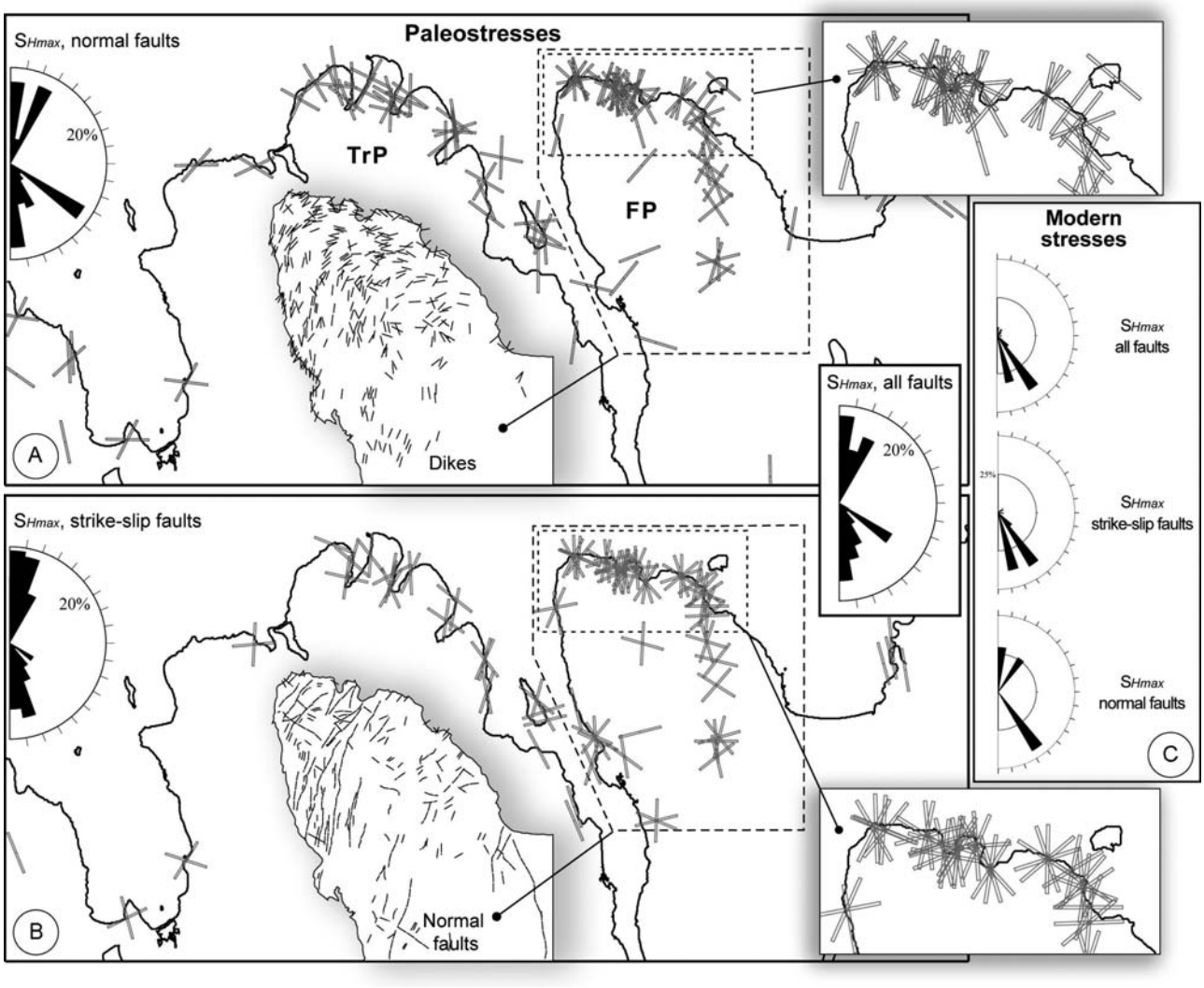

Figure 2. Paleostresses and modern stresses along the TFZ. (a and b) Maximal horizontal stress S_{Hmax} inferred from inversion of fault-slip data. Trends of dikes and trace of normal faults in the Flateyjarskagi peninsula [*Young et al.*, 1985] are also shown. (c) (S_{Hmax}) from focal earthquakes inversion. Rose diagrams illustrate the S_{Hmax} directions for stress states compatible with the right-lateral slip on the TFZ. Frequency in the direction is weighted with the number of faults. TrP and FP, Tröllaskagi and Flateyjarskagi peninsulas. Modern stresses are from *Garcia et al.* [2002], and paleostresses are from *Bergerat et al.* [1990, 1992, 2000], *Angelier et al.* [2000], and *Garcia et al.* [2002].

clockwise deviation. Treating separately strike-slip and normal regimes, the most important rotations of S_{Hmax} trends are found in the normal fault population, with 17% of the normal fault motions resulting from a N020°–030°E S_{Hmax}, whereas 18% result from a N120°–130°E S_{Hmax}. These two major deviations are clockwise and anticlockwise, respectively, relative to the N017°E trend of S_{Hmax} expected from simple consideration of the plate divergence direction (N107°E). The deviated trends correspond to maximal principal stresses S_{Hmax} almost perpendicular and parallel to the mean strike of the TFZ, respectively.

[17] A major difficulty while correlating paleostress states inferred from fault-slip data with the development of the TFZ is that the exact ages of the reconstructed paleostress states are unknown (within the bounds issued from the ages of the affected lava). However, the comparison between the paleostresses and the rift structures helps to formulate hypotheses. Fissures, dikes and normal faults along the Northern Volcanic Zone trend between N170°E and N010°E. If the S_{Hmax} directions within this range are discarded because they could result from rifting tectonics, the remaining major peaks of S_{Hmax} would trend 020°E–030°E (22%), 120°E–130°E (19%), and 160°E–170°E (18%). Stress states with S_{Hmax} almost parallel and perpendicular to the mean strike of the TFZ will thus account for more than 40% of the data.

[18] In order to identify the stress states that reflect the dextral shear along the TFZ, we compared the paleostress

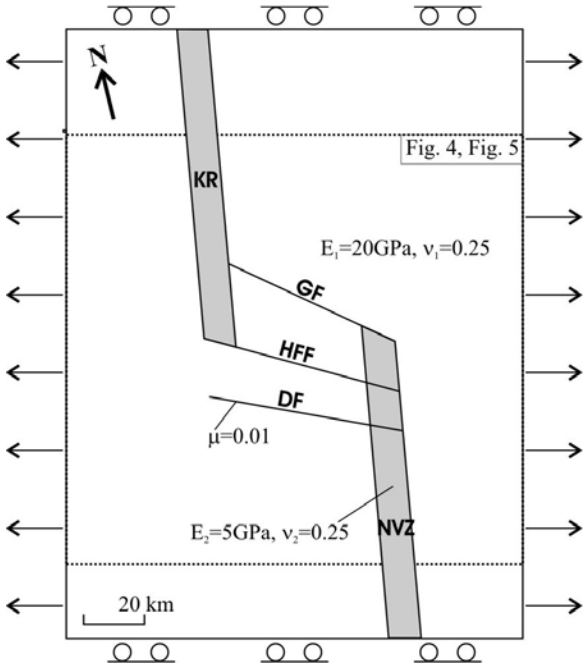

Figure 3. Model of the TFZ. The Kolbeinsey ridge (KR) and Northern Volcanic Zone (NVZ) are weak elastic strips with ν_2 Poisson ration and E_2 Young modulus, embedded in a strong elastic medium with ν_1 Poisson ratio and E_1 Young modulus. An in situ stress of 5 MPa simulates the horizontal component of the lithostatic stress field at ~600 m depth. The Dalvik (DF), Husavik-Flatey (HFF), and Grimsey (GF) faults follow a Mohr-Coulomb behavior with a μ friction. Lateral boundaries are moved away to simulate plate separation.

states with the major structures of the TFZ. A detailed study of these structures in the southern part of the TFZ has been conducted by *Young et al.* [1985]. These authors provided a detailed map of the dikes and normal faults within the eastern part of the block between the DF and HFF, in the Flateyjarskagi peninsula (Figure 2a and 2b). The direction of dikes and normal faults provides a rough estimate of the S_{Hmax} orientation. Dikes and normal faults draw a progressive clockwise rotation when approaching the HFF and thus reflect a curved stress field. *Young et al.* [1985] and *Jancin et al.* [1995] suggested that this change in the dike trend results from an increasing clockwise block rotations induced by dextral shear along the HFF. Although block rotations may exist, they cannot provide a viable mechanism to explain the variety in the dike strikes. For instance, near the HFF, dikes that trend almost perpendicular and dikes almost parallel to the HFF have the same 8 Ma age. Although local small block rotation may induce a bias, we regard the variety in dikes and faults strikes as the signature of a heterogeneous stress field, as previously claimed by *Fjäder et al.* [1994] and *Bergerat et al.* [2000].

[19] Dikes and normal faults mapped by *Young et al.* [1985] suggest that the stress field in the Flateyjarskagi peninsula is curved and discontinuous. From South to North, the S_{Hmax} direction progressively deflected from a N–S direction to a NNE–SSW direction when approaching the HFF. An abrupt change in stress directions occurs somewhere within the HFF, so that S_{Hmax} strikes WNW–ESE. Significantly, dikes that trend perpendicular and parallel to the HFF are both present along the fracture zone (Figure 2). It is quite remarkable that these two S_{Hmax} trends resemble the NNE–SSW and NW–SE S_{Hmax} inferred from fault-slip data inversion. They are thus likely representative of the stress states near the HFF. Because of the 8 Ma age of fault-parallel and fault-perpendicular dikes, we conclude that this stress field geometry characterized the very early history of the TFZ.

[20] In the northern part of the TFZ there is a dire lack of data, mainly because of its offshore location. However, a counterclockwise rotation of the rift fissure swarm, from N178°E to N160°E [*Bäckström and Gudmundsson*, 1989] certainly exists when passing from South to North the junction between the GF and the Northern Volcanic Zone. This deflection suggests that the stress field is not homogeneous near the eastern end of the GF.

[21] From all the above observations we conclude that the stress field during the development of the TFZ was characterized by an oblique horizontal stress trend with respect to the plate divergence direction. It is also shown that the S_{Hmax} trend was not homogeneous within the TFZ. Between the DF and HFF, S_{Hmax} exhibited a typical curved trajectory with a progressive northward clockwise rotation.

4. Modeling Stresses and Slip Along the TFZ

4.1. Model Configurations

[22] Numerical modeling has been conducted in order to evaluate how slip on major faults may control the stress field along the TFZ. A second aim of these experiments was to understand how fault interactions may influence the slip distribution in a BOT. Using the 2-D distinct element code UDEC [*Cundall*, 1980], we computed the horizontal stress between two en échelon ridges at 600 m depth. This depth is partly arbitrary but represents a reasonable approximation considering the average thickness of the lava pile eroded in the studied sites. Furthermore, changing this depth would not affect the conclusions of our modeling because the relative amount of slip along each fault and the type of stress deflections remain the same.

[23] In our numerical models, the Northern Volcanic Zone and the Kolbeinsey ridge are represented as NNE–SSW trending, 20 km wide stripes, with an offset of 120 km, embedded in an elastic medium (Figure 3). The thermal and lithospheric thickness contrast between the rift and off-rift zones is simulated by attributing different elastic parameters to each domain. The off-rift zones were given a Poisson ratio, ν_1, of 0.25 and a Young's modulus, E_1, of 20 GPa. These values are regarded as reasonable mean values of elastic constants in the Icelandic crust [*Palmason*, 1971]. A very low Young's modulus, E_2, was attributed to both the Kolbeinsey ridge and the Northern Volcanic rift, according to their nature as hot deforming zones with thin crust. Because the rift zone parameters are poorly constrained by real data, experiments with various E_2/E_1 ratios ranging

from 2 to 10 have been conducted. These experiments are not illustrated here because they revealed that changing the E_2/E_1 ratio had little effect on the stress deflections that we are interested in. These changes do not modify the sense and location of the stress rotations and simply affect their amounts.

[24] Regarding boundary conditions, the plate separation is simulated by moving away the lateral boundaries of the model. Three linear discontinuities representing the Dalvik (DF), Husavik-Flatey (HFF), and Grimsey (GF) faults link the two rift zones (Figure 3). They follow a Mohr-Coulomb behavior with zero cohesion, so that along-strike slip occurs if $\tau = \mu\sigma_n$, where τ and σ_n are the shear and normal stresses acting on the discontinuity while μ is the friction coefficient of the discontinuity. For models including several faults, we assumed that these faults have the same shear strength. Only experiments with very low friction coefficient ($\mu = 0.01$) are illustrated here, because the models with higher values produced unacceptable discrepancies between the simulated and actual stress fields.

[25] Because our plate model is 2-D, it does not take into account the vertical stress. Computing the full stress state would require a 3-D approach. This 2-D approach also neglects the vertical component of fault motion taken into account in analogical modeling [e.g., *Dauteuil et al.*, 2002; *Tentler*, 2007]; it is, however, sufficient to reproduce and interpret the stress deflections in the horizontal plane. Another simplification in our model deals with the shape of discontinuities: faults are treated as straight mechanical discontinuities that are continuous along strike. In the Tjörnes Fracture Zone, most actual faults in fact consist of en échelon fractures of various lengths. These fractures may be oblique to the general trend of the fault zone, which is the case for the Dalvik and Grimsey faults (Figure 1). Understanding the internal architecture of fault zones is beyond the scope of this paper, so that each major fault is regarded as a single discontinuity. We focus here on how the slip accumulation on crustal faults and the fault interactions may control the stress state along plate boundary.

[26] Because the age of initiation of the DF, HFF, and GF faults is unknown, we ran different kinds of models, the most typical ones being presented herein. The first type (single-fault model) involves a single fault crossing the TFZ. This fault may be the DF, HFF or GF, depending on the model, which aims at characterizing the behavior of each isolated discontinuity. The second type (multifault models) includes two or three faults, and thus principally aims at analyzing interactions between the DF, HFF and GF. All kinds of associations have been tested. Our models simulated a variety of internal configurations of the TFZ, the transform motion being accommodated by one, two or three faults. They thus represented possible configurations of the TFZ at different periods since the transform plate boundary initiated at 8 Ma, allowing consideration of synchronous or sequential development of the DF, HFF, and GF. A model without fault was also built for reference.

4.2. Elastic Models

[27] The first model in Figure 4a simulates the stress field between the Kolbeinsey ridge and the Icelandic rift in an oversimplified way. No fault exists in this model and plate separation is accommodated by elastic deformation between rift segments. This model was designed to serve as a reference in further comparisons with one-fault and multi-fault models. Not surprisingly, it suggests that large shear stress developed between the ends of the offset ridge segments prior to the transform fault development. Similar results were obtained by analytical calculation [*Pollard and Aydin*, 1984] and finite elements modeling [*Gudmundsson et al.*, 1993]. *Gudmundsson and Homberg* [1999] demonstrated that shear stress increases as plate separation continues. When the shear stress reaches the strength of the crust, faults develop and then relax the shear stress. Cycles of stress accumulation and release are necessary to produce a throughgoing transform fault connecting the two ridges.

[28] In our Kolbeinsey-Icelandic rift model (Figure 4a), the zone of shear stress concentration encompasses the whole TFZ. At this early stage, the three DF, HFF, and GF may develop because the stress condition for faulting is reached. In terms of stress orientation, this model shows that inside the future TFZ S_{Hmax} is not perpendicular to the direction of plate separation but trends N012–172°E, and locally N157°E. This stress deviation results in a significant decrease of the angle (originally 90°) between S_{Hmax} and the future DF, HFF, and GF, and hence involves more suitable conditions for slip to occur on these faults. It should be however noted that the predicted angle exceeds 30° and it may suggest that rocks friction could be smaller than that predicted by rock mechanics. Such high angles have effectively been observed on major transform faults, like the San Andreas Fault [e.g., *Townend and Zoback*, 2001].

4.3. Single-Fault Model

[29] The next models involved a single fault connecting the two ridges segments. Three models, referred to as DF (Figure 4b), HFF (Figure 4c) and GF (Figure 4d) models, have been elaborated in order to isolate the contribution of each fault to the stress pattern within the TFZ. The stress distribution in these single-fault models is quite different from that issued from the first, no-fault elastic model. This large difference indicates that fault zones bring major contribution to the near stress field in transform plate boundaries. In the TFZ, S_{Hmax} is approximately perpendicular to the plate divergence except in the vicinity of the active fault. The stress pattern is heterogeneous there and the deflection of the S_{Hmax} direction is maximal near the fault tips. The stress distribution is symmetrical relative to the fault center. In the two compressive quadrants near fault tips, S_{Hmax} is deviated anticlockwise whereas it rotates clockwise in the extensional quadrants. This curved stress pattern is typical of "isolated faults" [*Homberg et al.*, 2004].

[30] For right-lateral faults making a high angle to the far-field S_{Hmax}, like those of the TFZ, clockwise rotations are small. Anticlockwise rotations are much larger, especially in the HFF and GF models where they reach 70° and 55°, respectively (Figures 4c and 4d). These rotations result in a NW–SE to WNW–ESE maximal horizontal stress S_{Hmax} on average, a range well illustrated by inversions of both the

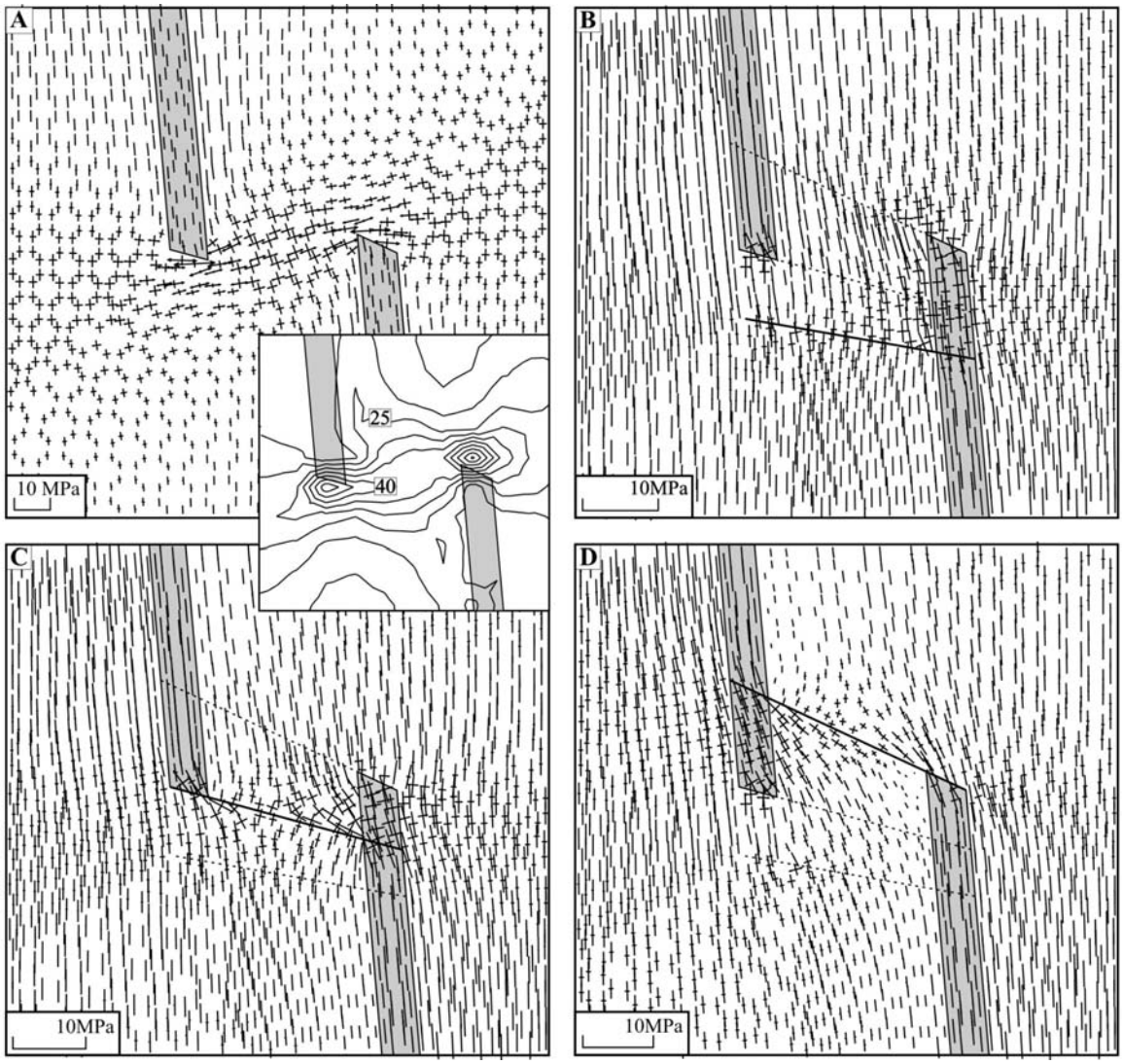

Figure 4. Stress states for elastic and single-fault models in the Tjörnes Fracture Zone. (a) No fault is included in model that simulates the proto-Tjörnes Fracture Zone (TFZ) before development of the Dalvik, Husavik-Flatey, and Grimsey faults. Inset shows the shear stress concentration (in MPa) between the two rifts. In single-fault models, the TFZ includes only one fault (thick line), either the (b) Dalvik, (c) Husavik-Flatey, or (d) Grimsey fault. Location of others faults is shown for reference as dashed line. Note that the stress field changes from one model to another.

paleofaults and the earthquake mechanisms (Figure 2). If both the GF and HFF models successfully simulate the importance of such a NW–SE direction, they imply different stress field geometry with the TFZ. Indeed, the place and amount of these anticlockwise rotations differ from one model to another. In the HFF, the maximum rotation occurs close to the HFF and more particularly near its northeastern corner. S_{Hmax} is almost parallel to the fault strike there, and thus explains the WNW–ESE dikes located exclusively near this fault.

[31] In the GF model, a similar fault-parallel compression occurs near the GF. Unfortunately, no stress data is available from this area, which precludes verification. It is however remarkable that the GF model does not simulate fault-parallel compression near the HFF. Because such a compression is attested by 8 Myr old dikes, this observation excludes the hypothesis of the GF being the main active structure during the initiation of the TFZ. This conclusion also applies for the DF. Not only does the HFF model simulate a fault-parallel compression, it also simulates other stress directions suggested by the geological field data. This model is discussed in more detail in section 4.4 and is compared with multifault models.

4.4. Multifault Model

[32] The last models are multifault models which include two faults or the three faults of the TFZ. A variety of two

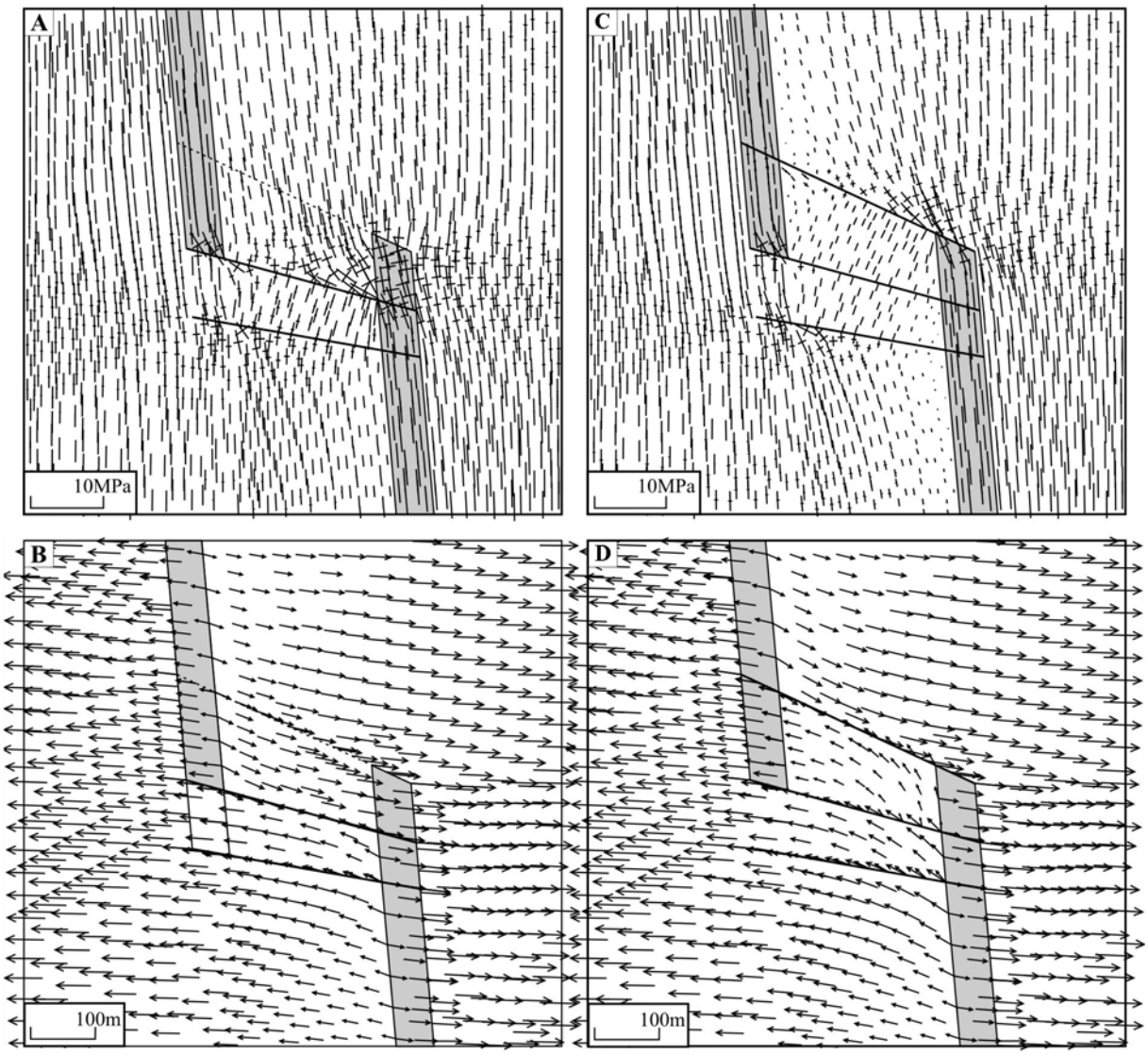

Figure 5. (a and c) Stress and (b and d) slip distribution in the TFZ for multifault models. In Figures 5a and 5b, the TFZ includes two plate boundary faults, the Dalvik and Husavik-Flatey faults. Location of the Grimsey Fault is shown for reference as dashed line. In Figures 5c and 5d, the TFZ includes the Dalvik, Husavik-Flatey, and Grimsey faults. Note that slip is allowed along all faults but only the most northern one accommodates plate motion. Fault interaction thus locks the Dalvik Fault (left) in the two fault model. In the three-fault model (right), both the Dalvik and Husavik-Flatey faults are locked.

fault models has been examined. The model where slip is allowed on both the HFF and DF best fits most of the geophysical and geological data. It is illustrated in Figure 5a. As discussed below, this preferred model suggests that the HFF is the major plate structure, probably since the initiation of the TFZ. Other multifault models reveal significant inconsistencies with the geological and geophysical data and thus do not represent acceptable internal configurations of the TFZ. One of these models, the DF-HFF-GF model, is however shown in Figure 5b for illustration.

[33] In the DF-HFF model, the stress state in the TFZ exhibits a complex stress pattern (Figure 5a). The description below applies for both the DF-HF (Figure 5a) and HFF (Figure 4c) models, because these models exhibit very similar stress fields. Inside the block between the DF and HFF and from South to North, S_{Hmax} progressively rotates clockwise from a N12°E to N34°E direction when approaching the HFF. This curvature in S_{Hmax} trends resembles that actually revealed by the dike trends (Figure 2). *Young et al.* [1985] suggested that dikes were originally trending N–S and that their present-day curved pattern results from clockwise block rotation induced by a dextral shear on a 11 km large zone, shear increasing close to the HFF. The lack of paleomagnetic data in Iceland precludes any reliable estimation of possible block rota-

tions. If our model is representative of the plate movement accommodation in the TFZ, the change in the strike of dikes should be regarded as primary and reflects the original configuration of the stress pattern. Although we cannot identify the type of stress regimes with our 2-D approach, the fault-perpendicular S_{Hmax} simulated near the HFF in our modeling experiments may likely correspond to a normal stress regime (at least locally). Typically, this S_{Hmax} direction is quite well represented among the normal paleostress regimes obtained from fault slip inversion and indicated by the observation of large-scale normal faults (Figure 2).

[34] Along the eastern half of the HFF, stresses rotates counterclockwise so that the minimum (S_{Hmin}) and maximum (S_{Hmax}) horizontal principal stresses trend almost perpendicular and parallel to the main fault strike, respectively. Such a stress state with fault-parallel compression (or fault-perpendicular extension) is demonstrated by the inversion of mesoscale strike-slip and normal faults and by the WNW–ESE dikes along the HFF and the small basin at the eastern ends of the HFF (Figure 2a and 2b).

[35] Other multifaults models show a much lower fit with the paleostress field and geological structures. As an example, the DF-HFF-GF model fails to replicate a S_{Hmax} fault-parallel compression near the HFF (Figure 5c). Among all single-fault and multifault models, the HFF and DF-HFF models show the best agreement with the data. Remarkably, although these two models are similar as far as the stress field geometry is concerned, they are quite different in terms of deformation within the TFZ due to fault interaction. In the DF-HFF model, the slip on the HFF induces locking of the DF where no strike-slip displacement occurs (Figure 5b). It is also the case when slip is also allowed on the GF (Figure 5d). Because slip on the GF or HFF inhibits activity along the DF and because the DF model (Figure 4b) does not fit the geological and geophysical data, we conclude that the DF has never been a major structure of the TFZ.

[36] The GF should also be regarded as a minor plate structure, at least during the early history of the TFZ (this will not be the case in the future, as suggested by its high level of seismicity). The hypothesis of a TFZ configuration with the GF accommodating most of the plate motion is unlikely because all models that include the GF did not fit geological data (see this paragraph and the previous one). In addition, large permanent slip on the GF would have locked the other two faults (see Figure 5d for example), which clearly was not the case of the HFF. The HFF is known to have accommodated at least 5 km and possibly up to 60 km of right-lateral displacement. Also, because of the discrepancies between the data and the predicted stress orientations, the GF cannot be considered as the master plate structure of the TFZ, in the past or even at the Present. However, significant seismic activity presently occurs along this fault and its significance in terms of plate boundary evolution will be discussed below.

5. Discussion and Conclusion

[37] Despite limitations, our 2-D distinct element experiments bring constraints regarding the slip distribution and the crustal stress field geometry within broad oceanic transforms (BOTs), based on the analysis of the Tjörnes Fracture Zone (TFZ). The multifault models (Figure 5), which include several subparallel faults, suggest that BOTs provide the fossil image of abandoned faults, rather than revealing synchronous major activity along their constitutive faults. The large finite width of BOTs thus results from slip transfer through time from one major fault to another. At each stage during the development of the transform system, the plate relative motion is not distributed along the plate boundary faults in a steady state manner. It rather concentrates along a single master fault, the other major fault zones remaining locked or with little activity.

[38] Transform models shown here were based on a specific plate configuration based on the TFZ, but the predicted accommodation of the plate transform movement and stress field show similarities with some observations on other BOTs. In contrast with typical oceanic transforms which consist in one narrow throughgoing valley that separates rift segments and concentrate shear stress, offset in BOTs is accomplished within a wide, complexly deformed area. BOTs are much common in fast spreading ridges, but also exist in slow and ultraslow spreading environment and their internal architecture is variable. They may consist of closely spaced transform faults trending almost parallel to the spreading direction and separating short accretionary zones, like the Quebrada and the Garret fracture zones that offset the fast spreading East Pacific Rise (Pacific-Nazca) and the Andrew Bain transform in Southwest Indian Ridge. Accretionary zones within the transform either follow the same trend as the main ridges like along the Qebrada fracture zone [*Searle*, 1983; *Lonsdale*, 1989] or may be very oblique to the spreading direction like in the Garret and Andrew Bain transforms [*Lonsdale*, 1989; *Sclater et al.*, 2005]. Other BOTs do not show any evidence of accretion like the Romanche transform and the TFZ that offset the slow spreading Mid-Atlantic Ridge. A last type of offset in large transforms is accomplished by antithetic strike-slip faults at high angle to the shear zone in a book-shelf manner like in the South Iceland Seismic zone (Mid-Atlantic [*Einarsson et al.*, 1981] or those described along the Cocos-Nazca plate boundary [*Bandy and Hilde*, 2000]. These different configurations probably reflect the various processes that favor excessive width of broad transforms such as the thermal structure of the lithosphere, change in plate motion, propagation of the spreading ridges, and inherited discontinuities [*Einarsson and Björnsson*, 1979; *Searle*, 1983; *Lonsdale*, 1989; *Dauteuil et al.*, 2002; *Ligi et al.*, 2002]. Collectively, these BOT are complexly built zone with numerous second-order structural elements. Several lines of evidences suggest that they are mobile belts and that their large observed widths, at least for BOTs of the first and second types described above, may result from a scenario implying successive fault abandonment and fault development. For example, the 900 km long and 100 km wide right-lateral Romanche transform fault includes two major valleys and the seismicity shows that the present-day plate motion occurs along the southern valley fault. The much thicker turbiditic sequence on the northern valley

suggests that it marks the former principal plate boundary that migrated a few million years ago on the southern valley fault [*Bonatti et al.*, 1994; *Ligi et al.* 2002]. In the same manner, the time reconstructions since 20 Ma by *Sclater et al.* [2005] of the 750 km long and 120 km large Andrew Bain transform implies a complex building of this transform zone, involving transient strike-slip faults and oblique accretion, prior structural elements being abandoned during the slipping history. Major reorganizations of the plate structures seem to correlate with changes, even small, in the direction of plate motion [e.g., *Lonsdale*, 1989; *Sclater et al.*, 2005]. Our modeling results suggest that fault interaction may be another factor that controls the activity within large transforms as slip on a fault may lock activity on adjacent faults. Although still poorly constrained, processes such as sealing or rheological change for faults governed by geochemical processes [*Wibberley*, 1999] may also likely contribute to the abandonment of faults in BOTs.

[39] As far as the slip distribution is concerned at each stage of their evolution, BOTs thus resemble classical oceanic transform zones where plate motion is accommodated along a single, possibly segmented, major plate structure. Despite this similarity, they differ as from time to time, the relative motion in a BOT may be transferred from the current master fault to another fault, with transition periods where both faults are active. Along the Romanche transform, although large shocks are confined along the southern valley fault, small ones occur along the northern valley fault [*Ligi et al.*, 2002].The predominance of a single fault thus does not exclude that a moderate activity persists along older structures of the plate boundary, so that the seismicity affects a wide area. Slip motion on abandoned/locked faults may be triggered by a large slip occurring on the neighboring active master fault, but such a slip would likely remain moderate or occasional. This process probably explains why rare but large earthquakes occur along the DF and GF, although the short seismological recording period cannot clearly document what fault of the TFZ underwent the majority of large earthquakes.

[40] Our models predict that directions of stresses in the transform zones largely deviate relative to that expected for the plate divergence. In one fault model, the stress progressively rotates when approaching the strike-slip fault and the most pronounced deviations results in a S_{Hmax} direction oblique to the transform zone (Figure 4). In the case of a left-lateral offset as that simulated here, the S_{Hmax} direction is rotated in a counterclockwise sense; it would occur in opposite way for a right-lateral offset. Such a stress rotation correlates well with the angular relationship observed in many BOTs between the normal faults scarps and general trend of the plate boundary [*Lonsdale*, 1989]. The stress pattern obtained in our models suggests that more abrupt and opposites changes in the direction of second-order tectonic structures may also exist but such deviations would be difficult to document in the deep marine BOTs. The emerged TFZ provides however a unique example to test this hypothesis. The stress field reconstructed from minor faults and earthquake focal mechanisms (Figure 2) shows stress rotations in both senses, in good agreement with the two-fault models (Figure 5a). We therefore suggest that slip on strike-slip faults in BOTs may induce a variability in the second-order element trend. In multifault model, besides stress deflections near the active master fault, stress directions within intrafault blocks differ from one block to another. Both the inactive faults and the master active fault of the BOT are thus responsible for mechanical decoupling between the blocks of the transform plate boundary resulting in a wide deflected stress field. In the ultimate configuration with three well developed faults (Figure 5a), the stress pattern is simpler and the S_{Hmax} direction makes a high angle with the plate faults, except in the vicinity of the active fault. If normal faulting is promoted, such stress orientation will result in normal faults trending almost perpendicular to the transform boundary. Such structures are well documented in the TFZ (Figure 2) and also exist along the Blanco transform, northeast Pacific ocean [*Dziak et al.*, 2000] and should be regarded has the signature of stress deviations. Our models also suggest that if the faults of the BOT differ in age, that is, if faults developed in sequence, the stress pattern changes in time as a function of the development sequence of individual faults. In this case, large changes in orientation may affect the stress field within the BOT during its history.

[41] As mentioned before, a common feature in BOTs is the occurrence of normal faults oblique to the spreading direction. Our 2-D models dot not allow to resolve the coexistence of normal and strike-slip faults in large transform zones but we speculate that fault interactions may induce changes in the stress magnitudes leading to stress permutations and thus encouraging either strike-slip or normal faulting in specific areas and in variable way during the slip history. This hypothesis is supported by the good agreement between the simulated S_{Hmax} pattern and the curvature of the normal faults within the DF-HFF block and the normal fault trends described above in other BOTs.

[42] In this paper, we considered the case of a BOT across which the plate motion has a slight extensional component, as a function of the limited obliquity of the BOT with respect to the direction of plate separation. The fault plate motion angle increases across the BOT from south to north, as a consequence of the differences in fault trends. Other plate configurations were not examined, but the stress orientation very likely depends on the fault plate motion angle and on the difference in strikes between the faults. The stress field within oceanic transforms should also likely be controlled by fault properties of the strike-slip discontinuities. Such phenomenon was documented for the Eltanin transform [*Beutel and Okal*, 2003], a classical transform cutting the south East Pacific Rise (Pacific-Antarctic) where strong asperities on otherwise strong faults bring heterogeneity in the stress field, including the development of large tensional stresses, enhancing normal faulting with anomalous focal geometry of earthquakes.

[43] As far as the TFZ is concerned, several conclusions and hypotheses can be drawn concerning the development order of each fault of the TFZ and their properties. First, the curved stress trajectory within the block between the DF

and HFF and the coexistence of both fault-perpendicular and fault-parallel compressions along the HFF were simulated in the model including the DF and HFF (Figure 5a). As this stress field is partly constrained by 8 Myr old dikes, it probably characterizes the stress state that prevailed during the initiation of the TFZ. The development of the DF and HFF was thus related to the initiation of the TFZ transform plate boundary and the DF is of similar age as, or slightly older than, the HFF. Although the age of initiation of the GF cannot be tightly constrained, this fault zone is undoubtedly a young plate boundary structure. Although we did not investigate plate configurations with different friction coefficients along the faults of the TFZ, the modeling results allow us to discuss the frictional strength of the DF, HFF, and GF. Paleostress studies along the HFF suggested that significant variations in frictions occurred, between situations of moderate friction and low friction [*Angelier et al.*, 2000]. The results of our modeling experiments also suggest low friction along active fault branches. The coexistence of both fault-perpendicular and fault-parallel compressions along the HFF even requires that the HFF has a very low friction coefficient, close to 0.01. This value is much lower than the 0.6–1.0 range for rock strength estimated from experimental data [*Byerlee*, 1978] and in situ stress measurements [*Townend and Zoback*, 2000], so that the HFF appears to be frictionally very weak. Fault friction is a complex property that may depend on many factors, and the frictional strength of major faults remains a controversial topic [e.g., *Scholz*, 2000; *Townend and Zoback*, 2001; *Carpinteri and Paggi*, 2005]. Our assumption of a low coefficient of friction is in agreement with some studies based on surface heat flow [*Lachenbruch and Sass*, 1980; *d'Alessio et al.*, 2006], thermochronology [*Xu and Kamp*, 2000; *d'Alessio et al.*, 2003], orientation of the maximum principal stress [*Mount and Suppe*, 1987; *Provost and Houston*, 2001; *Townend and Zoback*, 2004], which suggest that the average coefficient of friction of large active faults could be 0.2 or lower. However, using similar data, other authors argued that natural faults have frictional properties quite similar to laboratory measurements [*Scholz et al.*, 1979; *Townend and Zoback*, 2000; *Castillo and Hickman*, 2000].

[44] Whereas the HFF was (and may have persisted as) a weak fault structure, a low resistance of the three branches (DF, HFF, and GF) to present-day shear traction is unlikely. Whereas such a configuration would imply a widespread NNE–SSW trending S_{Hmax} within the TFZ (see Figure 5c), the modern stress field in fact shows a dominant NW–SE S_{Hmax} trend (Figure 2). The mechanism of faulting along the DF and GF with left-lateral slip on N–S faults that accommodate the dextral shear imposed by the plate motion argues for an immature stage of these two faults [*Bergerat and Angelier*, 1999, 2008]. The GF is not, at least until now, a throughgoing crustal discontinuity like the HFF and thus should be considered as a nonmature, possibly strong, fault. However, the GF has strong potential to become the master fault of the BOT in the future, as a result of the northward rift propagation of the active onland rift (i.e., the North Volcanic Zone of Iceland [*Gudmundsson et al.*, 1993]). This cannot be the case for the DF. Therefore, although no evidence exists that the activity of the present master fault (the Husavik-Flatey Fault) is decreasing, it is likely that in the future the main transform motion will be transferred to the Grimsey Lineament.

[45] **Acknowledgments.** Financial support was provided by the European Commission (contract EVR1-CT-1999-40002), the IPEV (Arctic Program 316) and by the French-Icelandic scientific-cultural collaboration program (Iceland Ministry of Education and Culture and French Ministère des Affaires Etrangères). We thank J.-F. Brouillet for help in drawing Figure 2. GMT software was used for some of the figures. Constructive reviews of two anonymous reviewers are gratefully acknowledged.

References

Angelier, J., F. Bergerat, and C. Homberg (2000), Variable coupling across weak transform fault: Flateyjarskagi, Iceland, *Terra Nova*, *12*, 97–101, doi:10.1046/j.1365-3121.2000.00279.x.

Angelier, J., R. Slunga, F. Bergerat, R. Stefansson, and C. Homberg (2004), Perturbation of stress and oceanic rift extension across transform faults shown by earthquake focal mechanisms in Iceland, *Earth Planet. Sci. Lett.*, *219*, 271–284, doi:10.1016/S0012-821X(03)00704-0.

Bäckström, K., and A. Gudmundsson (1989), The grabens of Sveinar and Sweinagja, NE Iceland, *Prof. Pap. 8901*, pp. 1–38, Nord. Volcanol. Inst., Reykjavík.

Bandy, W. L., and T. W. Hilde (2000), Morphology and recent history of the ridge propagator system located at 18°N, 106°W, *Spec. Pap. Geol. Soc. Am.*, *334*, 29–40.

Bergerat, F., and J. Angelier (1999), Géométrie des failles et régimes de contraintes à différents stades de développement des zones transformantes océaniques: Exemples de la zone sismique sud-islandaise et de la zone de fracture de Tjörnes (Islande), *C. R. Acad. Sci.*, *329*, 653–659.

Bergerat, F., and J. Angelier (2008), Immature and mature transform zones near a hot spot: The South Iceland Seismic Zone and the Tjörnes Fracture Zone (Iceland), *Tectonophysics*, *447*, 142–154, doi:10.1016/j.tecto.2006.05.046.

Bergerat, F., J. Angelier, and T. Villemin (1990), Fault system and stress pattern on emerged oceanic ridges: A case study in Iceland, *Tectonophysics*, *179*, 183–197, doi:10.1016/0040-1951(90)90290-O.

Bergerat, F., J. Angelier, and T. Villemin (1992), Déformations cassantes dans la partie émergée d'une zone transformante océanique; la zone de fractures de Tjörnes (Islande), *C. R. Acad. Sci., Ser. II*, *315*, 1011–1018.

Bergerat, F., J. Angelier, and C. Homberg (2000), Tectonic analysis of the Husavik-Flatey fault (northern Iceland) and mechanisms of an oceanic transform zone, the Tjörnes Fracture Zone, *Tectonics*, *19*, 1161–1177, doi:10.1029/2000TC900022.

Beutel, E. K., and E. A. Okal (2003), Strength asperities along oceanic transform faults: A model for the origin of extensional earthquakes on the Eltanin transform system, *Earth Planet. Sci. Lett.*, *216*, 27–41, doi:10.1016/S0012-821X(03)00484-9.

Bonatti, E. (1996), Origin of the large fracture zones offsetting the Mid-Atlantic Ridge, *Geotectonics*, Engl. Transl., *30*, 430–440.

Bonatti, E., M. Ligi, L. Gasperini, A. Peyve, Y. Raznitsin, and Y. J. Chen (1994), Transform migration and vertical tectonics at the Romanche fracture zone, equatorial Atlantic, *J. Geophys. Res.*, *99*, 21,779–21,802, doi:10.1029/94JB01178.

Burke, K., W. S. F. Kidd, and J. T. Wilson (1973), Relative and latitudinal motion of Atlantic hot spots, *Nature*, *245*, 133–137, doi:10.1038/245133a0.

Byerlee, J. D. (1978), Friction of rocks, *Pure Appl. Geophys.*, *116*, 615–626, doi:10.1007/BF00876528.

Carpinteri, A., and M. Paggi (2005), Size-scale effects on the friction coefficient, *Int. J. Solids Struct.*, *42*, 2901–2910, doi:10.1016/j.ijsolstr.2004.10.001.

Castillo, D. A., and S. H. Hickman (2000), Systematic near-field stress rotations adjacent to the Carrizo Plain segment of the San Andreas Fault, paper presented at 3rd Conference on Tectonic Problems of the San Andreas Fault System, Stanford Univ., Stanford, Calif., 6–8 Sept.

Cundall, P. A. (1980), UDEC: A generalised distinct element program for modelling jointed rock,/Peter Cundall Associates, *Rep. PCAR-1880*, Contract DAJA 37-39-C-0548, U.S. Army, Eur. Res. Off., London.

d'Alessio, M. A., C. F. Williams, and R. Bürgmann (2006), Frictional strength heterogeneity and surface heat flow: Implications for the strength of the creeping San Andreas Fault, *J. Geophys. Res.*, *111*, B05410, doi:10.1029/2005JB003780.

d'Alessio, M. A., A. E. Blythe, and R. Bürgmann (2003), No frictional heat along the San Gabriel fault, California: Evidence from fission-track thermochronology, *Geology*, *31*, 541–544, doi:10.1130/0091-7613(2003)031<0541:NFHATS>2.0.CO;2.

Dauteuil, O., O. Bourgeois, and T. Mauduit (2002), Lithosphere strength controls oceanic transform zone structure: Insights from analogue models, *Geophys. J. Int.*, *150*, 706–714, doi:10.1046/j.1365-246X.2002.01736.x.

DeMets, C., R. G. Gordon, D. F. Argus, and S. Stein (1994), Effect of recent revisions to the geomagnetic reversal tile scale on estimates of current plate motions, *Geophys. Res. Lett.*, *21*, 2191–2194, doi:10.1029/94GL02118.

Dziak, R. P., C. G. Fox, R. W. Embey, J. L. Nabelek, J. Braummiller, and R. A. Koski (2000), Recent tectonics of the Blaco Ridge, eastern Blanco transform fault zone, *Mar. Geophys. Res.*, *21*, 423–450, doi:10.1023/A:1026545910893.

Einarsson, P. (1991), Earthquake and present tectonics in Iceland, *Tectonophysics*, *189*, 261–279, doi:10.1016/0040-1951(91)90501-I.

Einarsson, P., and S. Björnsson (1979), Earthquakes in Iceland, *Joekull*, *29*, 37–43.

Einarsson, P., S. Björnsson, G. Foulger, R. Stefánsson, and T. Skaftadóttir (1981), Seismicity pattern in the South Iceland Seismic Zone, in *Earthquake Prediction: An International Review*, *Maurice Erwing Ser.*, vol. 4, edited by D. W. Simpson and P. G. Richards, pp. 141–151, AGU, Washington, D. C.

Fjäder, K., A. Gudmundsson, and T. Forslund (1994), Dikes, minor faults and mineral veins associated with a transform fault in north Iceland, *J. Struct. Geol.*, *16*, 109–119, doi:10.1016/0191-8141(94)90022-1.

Flovenz, O. G., and K. Gunnarsson (1991), Seismic crustal structure in Iceland and surrounding area, *Tectonophysics*, *189*, 1–17, doi:10.1016/0040-1951(91)90483-9.

Fox, P. J., and D. G. Gallo (1986), The geology of North Atlantic transform plate boundaries and their aseismic extensions, in *The Geology of North America*, vol. M, *The Western North Atlantic Region*, edited by P. R. Vogt and B. E. Tucholke, pp. 152–172, Geol. Soc. of Am., Boulder, Colo.

Garcia, S., and D. Dhont (2005), Structural analysis of the Husavik-Flatey transform fault and its relationships with the rift system in northern Iceland, *Geodin. Acta*, *18*, 31–41, doi:10.3166/ga.18.31-41.

Garcia, S., J. Angelier, F. Bergerat, and C. Homberg (2002), Tectonic analysis of an oceanic transform fault zone based on fault-slip data and earthquake focal mechanisms: The Husavik-Flatey Fault zone, Iceland, *Tectonophysics*, *344*, 157–174, doi:10.1016/S0040-1951(01)00282-7.

Garcia, S., N. Arnaud, J. Angelier, F. Bergerat, and C. Homberg (2003), Rift jump process in Northern Iceland since 10 Ma for $^{40}Ar/^{39}Ar$ geochronology, *Earth Planet. Sci. Lett.*, *214*, 529–544, doi:10.1016/S0012-821X(03)00400-X.

Grønlie, G., M. Chapmann, and M. Talwani (1979), Jan Mayen Ridge and Icelandic Plateau: Origin and evolution, *Nor. Polarinst. Skr.*, *170*, 25–47.

Gudmundsson, A. (1993), On the structure and formation of fractures zones, *Terra Nova*, *5*, 215–224, doi:10.1111/j.1365-3121.1993.tb00252.x.

Gudmundsson, A., and C. Homberg (1999), Evolution of stress fields and faulting in seismic zones, *Pure Appl. Geophys.*, *154*, 257–280, doi:10.1007/s000240050229.

Gudmundsson, A., S. Brynjolfsson, and M. T. Jonsson (1993), Structural analysis of transform fault-rift zone junction in north Iceland, *Tectonophysics*, *220*, 205–221, doi:10.1016/0040-1951(93)90232-9.

Homberg, C., J. Angelier, F. Bergerat, and O. Lacombe (2004), Using stress deflections to identify past ruptures in fault systems, *Earth Planet. Sci. Lett.*, *217*, 409–424, doi:10.1016/S0012-821X(03)00586-7.

Jancin, M., K. D. Young, B. Voight, and N. I. Orkan (1995), Dikes, minor faults and mineral veins associated with the transform fault in north Iceland, Discussion, *J. Struct. Geol.*, *17*, 1627–1631, doi:10.1016/0191-8141(95)00073-M.

Johnsson, G. L. (1974), Morphology of the mid-ocean ridge between Iceland and the Arctic, in *Geodynamics of Iceland and the North Atlantic Area*, edited by L. Kritjansson, pp. 49–62, D. Reidl, Norwell, Mass.

Kodaira, S., R. Mjelde, K. Gunnarsson, H. Shiobara, and H. Shimamura (1998), Evolution of oceanic crust on the Kolbeinsey ridge, north of Iceland, over the past 22 My, *Terra Nova*, *10*, 27–31, doi:10.1046/j.1365-3121.1998.00166.x.

Lachenbruch, A. H., and J. H. Sass (1980), Heat flow and energetics of the San Andreas Fault zone, *J. Geophys. Res.*, *85*, 6185–6223, doi:10.1029/JB085iB11p06185.

Ligi, M., E. Bonatti, L. Gasperini, and A. N. B. Poliakov (2002), Oceanic broad mutifault transform plate boundaries, *Geology*, *30*, 11–14, doi:10.1130/0091-7613(2002)030<0011:OBMTPB>2.0.CO;2.

Lonsdale, P. (1989), Segmentation of the Pacific-Nazca spreading center, 1°N–20°S, *J. Geophys. Res.*, *94*, 12,197–12,225, doi:10.1029/JB094iB09p12197.

Mauduit, T., and O. Dauteuil (1996), Small-scale models of oceanic transform zones, *J. Geophys. Res.*, *101*, 20,195–20,209, doi:10.1029/96JB01509.

McMaster, R. L., J.-G. E. Schilling, and P. R. Pinet (1977), Plate boundary within the Tjörnes Fracture Zone on northern Iceland's insular margin, *Nature*, *269*, 663–668, doi:10.1038/269663a0.

Mount, V. S., and J. Suppe (1987), State of stress near the San Andreas Fault: Implications for wrench tectonics, *Geology*, *15*, 1143–1146, doi:10.1130/0091-7613(1987)15<1143:SOSNTS>2.0.CO;2.

Palmason, G. (1971), Crustal structure of Iceland from explosion seismology, *Visindafelag Isl.*, *40*, 1–187.

Pollard, D. D., and A. Aydin (1984), Propagation and linkage of oceanic ridge segments, *J. Geophys. Res.*, *89*, 10,017–10,028, doi:10.1029/JB089iB12p10017.

Provost, A.-S., and H. Houston (2001), Orientation of stress field surrounding the creeping section of the San Andreas Fault: Evidence of a narrow mechanically weak fault zone, *J. Geophys. Res.*, *106*, 11,373–11,386, doi:10.1029/2001JB900007.

Riedel, C., M. Schmidt, R. Botz, and F. Theilen (2001), The Grimsey hydrothermal field offshore North Iceland: Crustal structure, faulting and related gas venting, *Earth Planet. Sci. Lett.*, *193*, 409–421, doi:10.1016/S0012-821X(01)00519-2.

Rögnvaldsson, S. T., A. Gudmundsson, and R. Slunga (1998), Seismotectonic analysis of the Tjörnes Fracture Zone, an active transform fault in north Iceland, *J. Geophys. Res.*, *103*, 30,117–30,129, doi:10.1029/98JB02789.

Saemundsson, K. (1974), Evolution of the axial rifting zone in northern Iceland and the Tjörnes Fracture Zone, *Geol. Soc. Am. Bull.*, *85*, 495–504, doi:10.1130/0016-7606(1974)85<495:EOTARZ>2.0.CO;2.

Scholz, C. (2000), Evidence for a strong San Andreas Fault, *Geology*, *28*, 163–166, doi:10.1130/0091-7613(2000)28<163:EFASSA>2.0.CO;2.

Scholz, C. H., J. Beavan, and T. C. Hanks (1979), Frictional Metamorphism, Argon Depletion, and Tectonic Stress on the Alpine Fault, New Zealand, *J. Geophys. Res.*, *84*, 6770–6782, doi:10.1029/JB084iB12p06770.

Sclater, J. G., N. R. Grindlay, J. A. Madsen, and C. Rommevaux-Jestin (2005), Tectonic interpretation of the Andrew Bain transform fault: Southwest Indian Ocean, *Geochem. Geophys. Geosyst.*, *6*, Q09K10, doi:10.1029/2005GC000951.

Searle, R. C. (1983), Multiple, closely spaced transform faults in fast-slipping fracture zones, *Geology*, *11*, 607–610, doi:10.1130/0091-7613(1983)11<607:MCSTFI>2.0.CO;2.

Sempéré, J.-C., P. Blondel, A. Brais, T. Fujiwara, L. Géli, N. Isezaki, J. E. Pariso, L. Parson, P. Patriat, and C. Rommevaux (1995), The Mid-Atlantic Ridge between 29°N and 31°30′N in the last 10 Ma, *Earth Planet. Sci. Lett.*, *130*, 45–55, doi:10.1016/0012-821X(94)00259-2.

Small, C., J. R. Cochran, J.-C. Sempéré, and D. Christie (1999), The structure and segmentation of the Southeast Indian Ridge, *Mar. Geol.*, *161*, 1–12, doi:10.1016/S0025-3227(99)00051-1.

Tentler, T. (2007), Focused and diffuse extension in controls of ocean ridge segmentation in analogue models, *Tectonics*, *26*, TC5008, doi:10.1029/2006TC002038.

Townend, J., and M. D. Zoback (2000), How faulting keeps the crust strong, *Geology*, *28*, 399–402, doi:10.1130/0091-7613(2000)28<399:HFKTCS>2.0.CO;2.

Townend, J., and M. D. Zoback (2001), Implications of earthquake focal mechanisms for the frictional strength of the San Andreas Fault system, in *The Nature and Tectonic Significance of Fault Zone Weakening*, edited by R. E. Holdsworth et al., *Geol. Soc. Spec. Publ.*, *186*, 13–21.

Townend, J., and M. D. Zoback (2004), Regional tectonic stress near the San Andreas Fault in central and southern California, *Geophys. Res. Lett.*, *31*, L15S11, doi:10.1029/2003GL018918.

Vogt, P. R., G. L. Johnson, and L. K. Kristjansson (1980), Morphology and magnetic anomalies north Iceland, *J. Geophys.*, *47*, 67–80.

Wibberley, C. (1999), Are feldspar-to-mica reactions necessarily reaction-softening processes in fault zones?, *J. Struct. Geol.*, *21*, 1219–1227, doi:10.1016/S0191-8141(99)00019-X.

Wilson, T. J. (1965), A new class of faults and their bearing on continental drift, *Nature*, *207*, 343–347, doi:10.1038/207343a0.

Xu, G., and P. Kamp (2000), Tectonics and denudation adjacent to the Xianshuihe Fault, eastern Tibetan Plateau: Constraints from fission track thermochronology, *J. Geophys. Res.*, *105*, 19,231–19,251, doi:10.1029/2000JB900159.

Young, K. D., M. Jancin, B. Voight, and N. I. Orkan (1985), Transform deformation of Tertiary rocks along the Tjörnes Fracture Zone, *J. Geophys. Res.*, *90*, 9986–10,010, doi:10.1029/JB090iB12p09986.

J. Angelier, Géosciences Azur, UMR 6526 CNRS-UNSA-UPMC-IRD, Observatoire Océanologique, B.P. 48, F-06235 Villefranche-sur-Mer CEDEX, France.

F. Bergerat and C. Homberg, ISTeP, UMR 7193, Université Pierre et Marie Curie, CNRS Case 129, 4 place Jussieu, F-75252 Paris CEDEX 05, France. (catherine.homberg@upmc.fr)

S. Garcia, Institut für Geologische Wissenschaften, Freie Universität Berlin, Malteserstrasse 74-100, D-12249 Berlin, Germany.